Electrical and Electronic Engineering 2014, 4(4): 73-79
DOI: 10.5923/j.eee.20140404.02

Absorption Bandwidth-Enhanced Metamaterial Absorber Using In-planed ELC Resonator and Cut-Wire

H. M. Lee

Department of Electronic Engineering, Kyonggi University, Suwon, Korea

Abstract In this paper, we present the design, fabrication, and characterization of a broadband metamaterial (MM) absorber, which consists of a lumped-resistor-loaded electric-inductive-capacitive (ELC) resonator and a cut-wire strip on the same side of the dielectric substrate. A metallic pattern layer of the proposed absorber is designed in parallel to the incident wave propagation direction. In contrast to a common ELC resonator, the lumped-resistor-loaded ELC resonator exhibits a switchable resonant mode behavior, thereby exhibiting a negative effective permeability ($\mu_{eff} < 0$). In addition, this resonator exhibits a low quality (Q)-factor owing to the loaded lumped resistors, which enhances the absorption bandwidth of an MM resonator. Our experiments showed that the proposed absorber exhibits a peak absorption rate of 91% at 8.87 GHz, and 2.8 GHz of a full-width at half-maximum (FWHM) bandwidth is achieved.

Keywords Absorber, Cut-Wire, Effective Medium, Electric-Inductive-Capacitive (ELC) Resonator, Metamaterial

1. Introduction

Meatamaterials (MMs) can be represented by the complex values of electric permittivity ε_{eff} ($= \varepsilon' + j\varepsilon''$) and magnetic permeability μ_{eff} ($= \mu' + j\mu''$). These complex values can be independently controlled by varying the dimensions of the electric and magnetic components. Additionally, the impedance of an MM can be well-matched to that of free space by tuning the electric and magnetic resonances. As a result, 100% absorption can be theoretically achieved. The configuration of the previously reported MM absorbers can be categorized into two types: absorbers with a metallic backing plate and metallic backplane-less absorbers. Most of the MM absorbers are equipped with a metallic backing plate [1–5] to avoid power transmission on the other side of the absorbers. However, the presence of backing plates is disadvantageous in stealth and camouflage applications [6]. The configuration of the previously reported metallic backplane-less MM absorbers involves the realization of two metallic patterns with the negative real parts of permittivity and permeability. The two metallic pattern layers separated by a dielectric spacer are designed orthogonally to the electromagnetic (EM) wave propagation direction [7–11]. In this case, the radar cross-section (RCS) of the metallic pattern expands at frequencies other than the targeted absorption frequency bands. Therefore, there is a need for a metallic pattern layer of the MM absorber to be designed in parallel to the EM wave propagation direction to avoid this problem. In our previous study, an MM absorber was designed by combining two open complementary split-ring resonators (OCSRRs) with a split-ring-resonator (SRR) separated by a dielectric substrate, and the metallic pattern layers were designed in parallel to the EM wave propagation direction [12]. Although, this structure serves as a dual-band MM absorber in the microwave frequency region, the absorption bandwidth of this MM absorber is quite narrow. This narrow bandwidth characteristic limits the absorber applications. Considering the fact that lumped elements can be used for enhancing the resonance bandwidth of an MM resonator [13], we present a new type of an MM absorber. The proposed MM absorber, which is designed by combining a lumped-resistor-loaded electric-inductive-capacitive (ELC) resonator and a cut-wire strip on the same side of the dielectric substrate, exhibits a broadband absorption characteristic. The proposed MM absorber structures are simulated using 3D field simulation tool, CST MWS (Micro Wave Studio).

2. Operating Modes of ELC Resonators

An ELC resonator, which does not require continuous electrical connections between the unit cells, was first proposed as an alternative to a thin metallic wire, and it strongly couples to a uniform electric field [14]. This ELC resonator structure is composed of two SRRs positioned back to back. A variant ELC resonator structure comprises two capacitive gaps on the exterior of an inductive arm [15]. Both the ELC resonators, unlike SRRs, possess a high level

* Corresponding author:
hmlee@kyonggi.ac.kr (H. M. Lee)
Published online at http://journal.sapub.org/eee
Copyright © 2014 Scientific & Academic Publishing. All Rights Reserved

of symmetry and do not exhibit a magneto-electric coupling behavior. With regard to the equivalent circuit, the ELC resonator can be considered as an *LC* circuit, where *L* and *C* are the geometric inductance and capacitance of the ELC structure, respectively. The incident EM field induces parallel and antiparallel magnetic dipoles in the two individual SRRs in each unit cell of the circuit, which correspond to symmetric and anti-symmetric modes, respectively [16].

Figure 1 illustrates the schematic and equivalent circuit of the two ELC resonators for symmetric and anti-symmetric modes. In the symmetric mode, the induced surface current components on the middle capacitive arm are out of phase, as shown in Figure 1(a). Therefore, the induced surface currents circulate around the outer edges of the ELC resonator. The symmetric mode originates from the magnetic coupling to the resonator, in which the effective permeability can be negative ($\mu_{eff} < 0$). However, in the case of the ELC resonator comprising two SRRs positioned back to back, the effective permeability is not negative (loop current mode). In the anti-symmetric mode, the induced surface current components on the middle capacitive or inductive arm are in phase, as shown in Figure 1(b). Therefore, the induced surface currents almost converge on the middle capacitive or inductive arm owing to the strong electric coupling, which contributes to the negative effective permittivity ($\varepsilon_{eff} < 0$).

3. MM Absorber Design with In-planed Resonators

We have designed an in-planed MM absorber by combining an ELC resonator and a cut-wire strip on the same side of the dielectric substrate, as shown in Figure 2(a), and simulations are carried out. The ELC resonators comprise a single metallic pattern layer etched on a Rogers R4003C dielectric substrate, which has a relative dielectric constant ε_r of 3.37, loss tangent δ of 0.003, and thickness t1 of 1.5 mm. Copper, with a conductivity σ of 5.8×10^7 S/m, is used for designing the metallic patterns. In the simulations, the incident EM wave illuminates the proposed MM absorber with a parallel polarization, where the magnetic field *H* being normal to the ELC resonator and the electric field *E* coupled to the capacitive element, as shown in Figure 2(a).

The periodic boundary conditions are applied to the top, bottom and two side walls of the waveguide. The other two opposite sides of the waveguide is assigned as open-waveguide ports, as shown in Figure 2(b). The lumped-resistor-loaded in the ELC resonator changes the resonance characteristics of the MM absorber. We simulate the proposed MM absorber structure for various values of the lumped resistors loaded within the ELC resonator to derive the optimum resistor value *R*, and the simulated impedance loci of the MM absorber over a frequency range of 8–12 GHz are shown in Figure 3. The marker numbers inside the impedance loci on the Smith chart indicate the points where the frequency is 8.95 GHz for various values of the lumped resistors loaded within the ELC resonator. When the lumped resistor value R = 910Ω, the input impedance of the proposed MM absorber is 371–j8 at 8.95 GHz. This impedance of the proposed MM unit cell is well-matched to that of free space (≈ 377Ω). When the lumped resistor value R > 910Ω, the quality (Q) factor of the ELC resonator will further reduce. However, the resonator is over-coupled to free space.

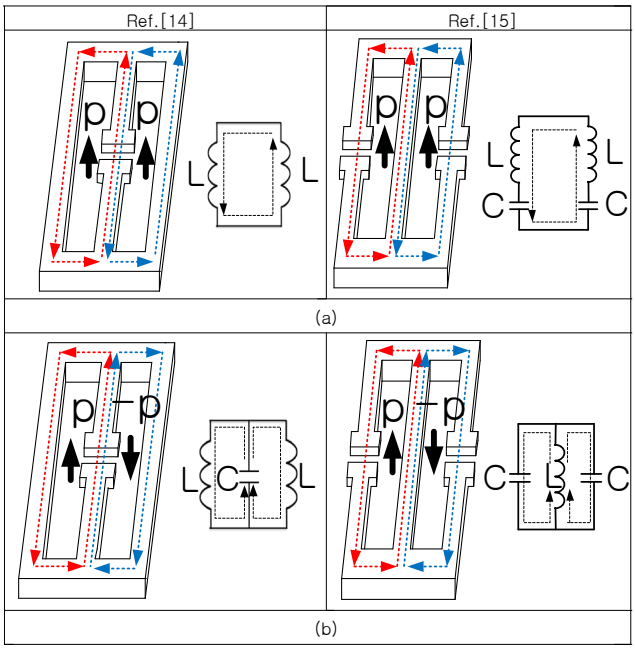

Figure 1. Schematic and its equivalent circuit of an ELC resonator. (a) Symmetric mode. (b) Anti-Symmetric mode. The arrows (black color) in the ELC resonator indicate parallel or anti-parallel dipoles by inducing circulate surface currents (red and blue color)

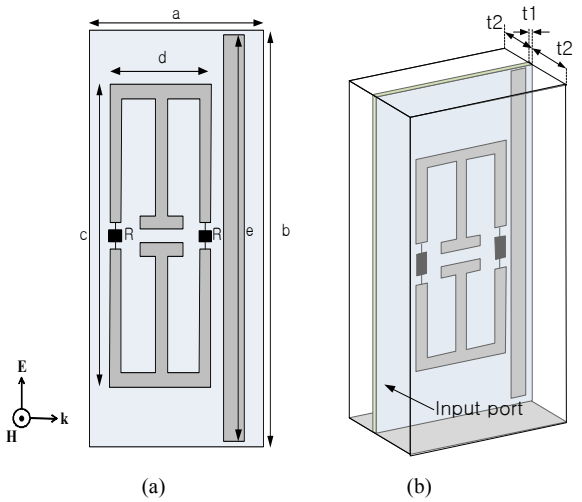

Figure 2. (a) In-planed MM absorber unit cell consists of an ELC resonator and a cut-wire strip with following geometric dimensions: a= 4.3 mm, b= 9.2 mm, c=6.9 mm, d= 2.5mm, e=9.0 mm, t1= 1.5 mm, t2=1.5 mm and R=910 ohm. (b) Simulation set-up

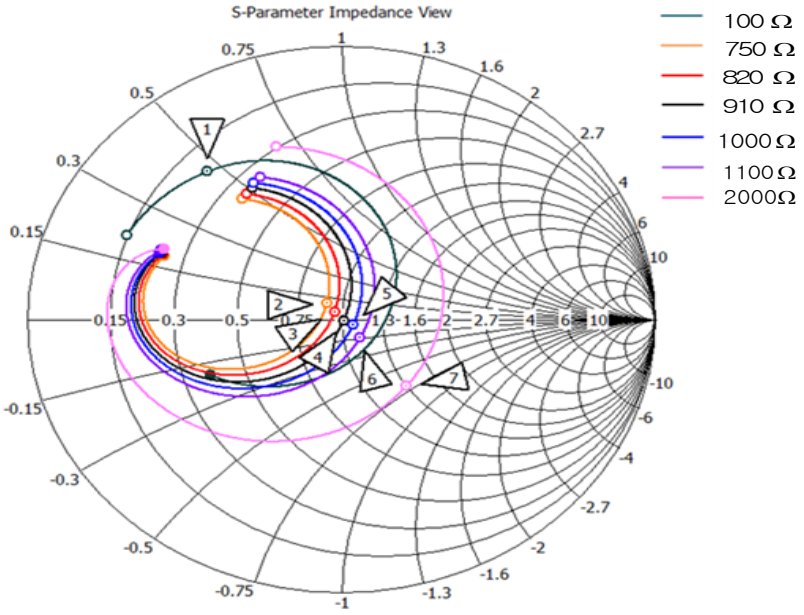

Figure 3. Simulated input impedance loci for various values of the lumped resistors loaded within the ELC resonator

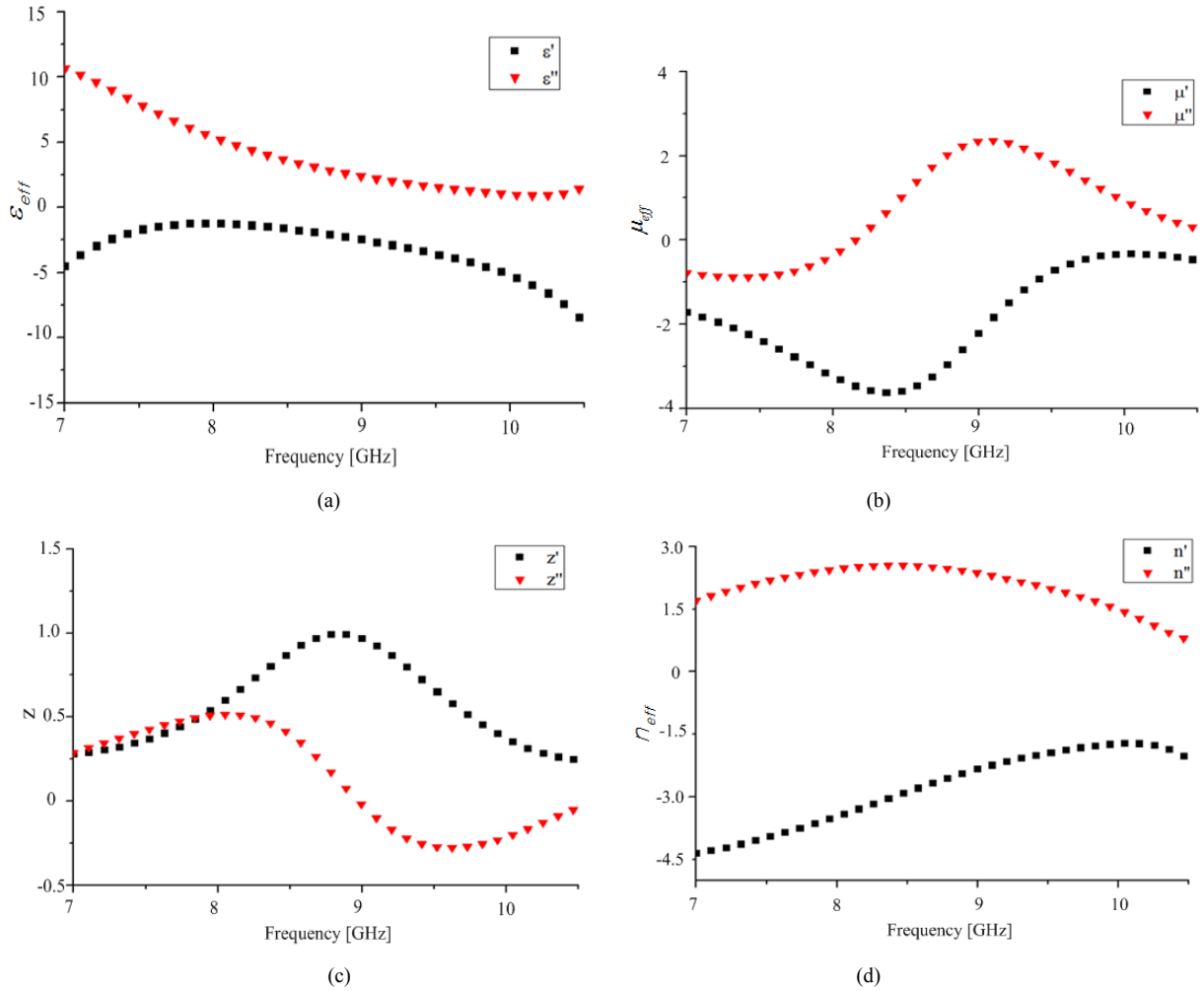

Figure 4. Effective medium parameters of the MM absorber extracted from the scattering parameters: (a) effective permittivity, (b) effective permeability, (c) normalized impedance and (d) effective refractive index

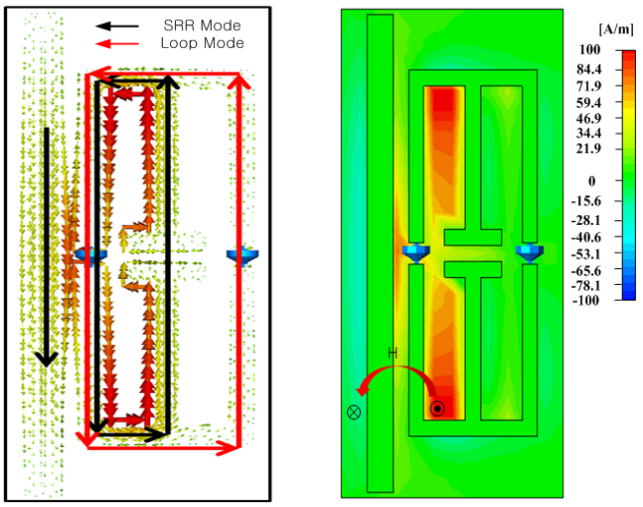

(a) (b)

Figure 5. Simulation results for the MM absorber at resonant frequency of 8.95 GHz: (a) surface current distribution and (b) magnetic field distribution

The scattering parameters of this MM unit cell are simulated, and the extracted effective medium parameters of the MM absorber under plane-wave incidence over a frequency range of 7.0–10.5 GHz are plotted as shown in Figure 4. The real and imaginary components of ε_{eff} (= $\varepsilon' + j\varepsilon''$) and μ_{eff} (= $\mu' + j\mu''$) are plotted as shown in Figures 4 (a) and (b), respectively. It should be noted that the real components of both the effective permittivity and permeability (ε' and μ') are negative and the imaginary components (ε'' and μ'') are positive, at 8.95 GHz. This aspect meets the general condition for the power flow and phase velocity directed in the opposite direction, which is expressed as $\varepsilon'\mu'' + \mu'\varepsilon'' < 0$ [17]. As a result, the proposed unit cell can be considered as a double-negative MM absorber unit cell. As shown in Figure 4 (c), the normalized impedance is near unity at a frequency of 8.95 GHz, which implies that the impedance of the proposed MM absorber unit cell is well-matched to that of free space. As shown in Figure 4 (d), the unit cell has a negative real part of the refractive index near its resonant frequency of 8.95 GHz. The negative sign of the real part of the refractive index indicates the phase velocity direction in a left-handed (LH) medium. The imaginary part of the refractive index (n″) is 2.39 at a frequency of 8.95 GHz, which denotes the absorption of the EM wave energy. As a result, the proposed structure functions as a broadband MM absorber.

Figure 5 shows the simulated surface current distribution and magnetic field distribution at the resonant frequency of 8.95 GHz. As shown in Figure 5(a), the current distributions of the ELC resonator can be divided into two parts: circular current path in a single SRR (SRR mode) and circular current path around the outer edges of the ELC resonator (loop mode) owing to the switchable resonant mode behaviour [18]. The induced magnetic dipole moments of the SRR and the loop are in parallel; however, the strength of the magnetic dipole moment of the loop is weaker than that of the SRR, thereby exhibiting a negative effective permeability ($\mu_{eff} < 0$).

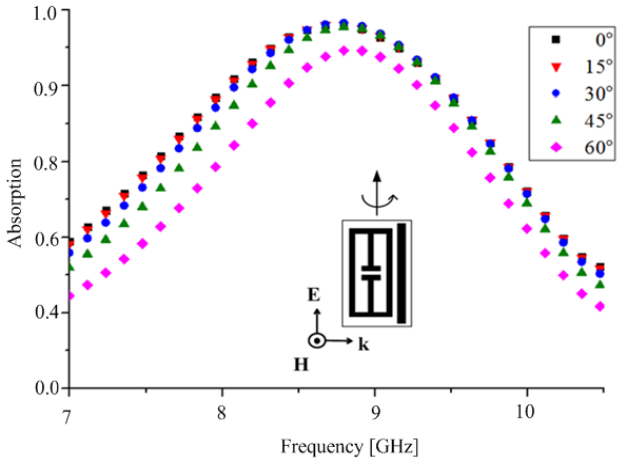

(a)

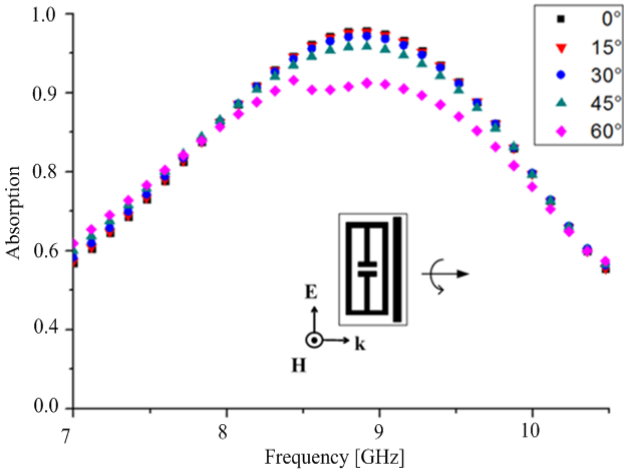

(b)

Figure 6. Simulated results of the absorption curve for oblique incident angle dependence: (a) TE polarization Surface current distribution and (b) TM polarization

The magnetic field generated from the ELC resonator is coupled to the cut-wire, as shown in Figure 5(b), which generates parallel surface currents in both the cut-wire and neighbouring metallic arm of the ELC resonator. These two parallel currents exhibit a negative effective permittivity ($\varepsilon_{eff} < 0$). As a result, the proposed structure functions as a double-negative MM absorber. Figure 6 shows the simulated absorption curve for TE and TM polarized incident of EM waves at the different angles. As the incidence angles increases, the peak absorption remains at 95% at an angle of 45°. Both the TE and TM polarization, it decreases to 84% and 79% at an angle of 60°, respectively. This decrease in the absorption can be explained on the basis of the fact that the incident magnetic field can no longer effectively drive the circulating currents in the ELC resonator's metallic patterns. The absorption characteristic can be observed from Figure 7, which shows the simulated distribution of the average power loss densities in the absorber unit cell at the peak absorption frequency of 8.95

GHz. It is noted that the power loss mainly occurs in the two lumped resistors of the ELC resonator and near the two outer edges of the metallic cut-wire, as shown in Figure 7. In case of the MM absorber with an ELC resonator without lumped resistors and a cut-wire configuration, power loss mainly occurs in the space near the capacitor plates of the ELC resonator and near the two outer edges of the metallic cut-wire.

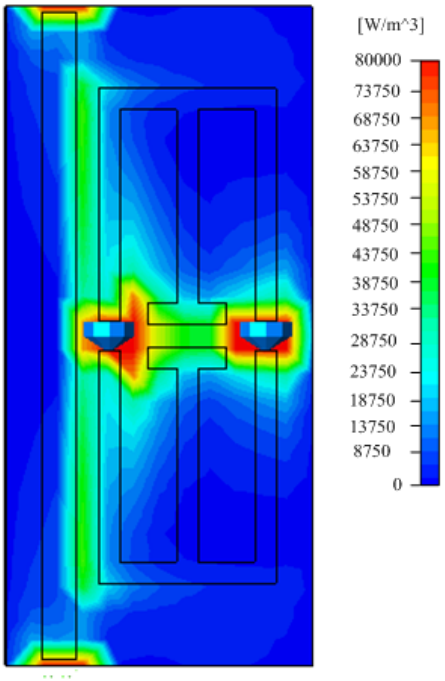

Figure 7. Distributions of average power loss density in the proposed MM absorber

4. Comparison of Different Types of MM Absorbers

To compare the effects of lumped resistors in ELC resonator, three different configurations of the in-planed MM absorbers are numerically investigated, as shown in Figure 8. The simulated results are listed in Table 1. For comparison purpose, an in-planed MM absorber with an ELC and a cut-wire (Type 1) is designed. In Type 3, single SRR is used in place of the ELC whereas the dielectric substrate is removed from the edges of the ELC in Type 2.

Table 1. Comparison of the simulation results of MM absorbers with different configurations

Specification	In-planed MM Absorber Structures		
	Type 1	Type 2	Type 3
a [mm]	4.1	4.3	3.4
b [mm]	7.4	9.2	10.2
Resonant Frequency [GHz]	9.08	8.95	9.09
Peak Absorption [%]	94	95	96
FWHM Bandwidth [GHz]	8.92-9.26	7.27-10.45	7.83-12.1

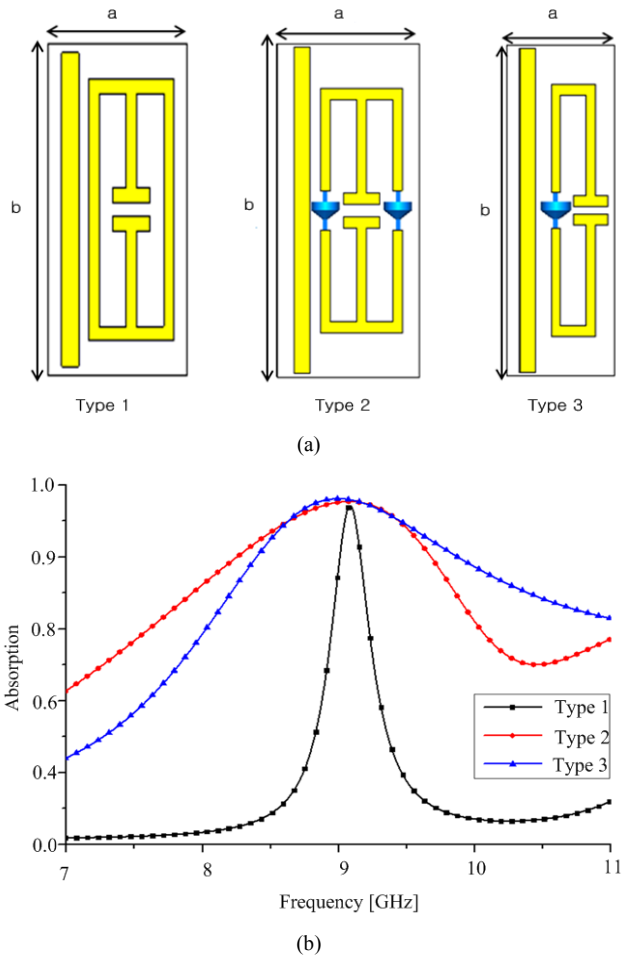

Figure 8. Simulated results for three different MM absorbers: (a) three different types of in-planed MM absorbers and (b) comparison of absorption for three different MM absorbers

The dimensions of the Type 1 are changed accordingly to keep their resonance at around 9.08 GHz. Table 1 compares the simulated absorption and full-width at half-maximum (FWHM) bandwidth of Types 1–3 at their simulated resonance frequency, respectively. From both simulated absorption values against frequency, it is found that the achieved peak absorption values slightly changes around 9 GHz frequency bands where the designs realized impedance matching. Types 2 and 3 have the broader FWHM due to the influences of the lumped-resistor on the ELC resonator which are lowering the Q-factor of the resonator.

5. Measurement Results

We have fabricated a prototype MM absorber sample for an experiment to verify the effectiveness of the MM absorber. The photographs of the fabricated single-layer metallization MM absorber strip samples are shown in Figure 9 (a). The sample is etched on a Rogers R4003C substrate using standard photolithography techniques. The lumped resistors (resistance R = 910 Ω, 1005-type thick film with a size of 1.0 × 0.5 mm) are loaded on the inductive arms of the ELC

resonators by applying the surface-mount soldering technology. A single period of the absorber strip consists of 70 unit cells etched on one side of a dielectric substrate. The absorber strips, each of which comprises an ELC resonator and a cut-wire strip configuration, are vertically aligned in parallel to the wave propagation direction. The inter-element spacing between the two vertically aligned absorber strips is set to 3 mm, and a silicon rubber substrate which has a relative dielectric constant ε_r of 3.37, and loss tangent δ of 0.001 is inserted between the absorber strips. The total size of the planar absorber with a planar array of absorber unit cells (33 × 70) is 312 × 303.6 mm. We have experimentally verified the behaviour of the absorber by measuring the S-parameters of the planar array of unit cells. Measurements are performed over a frequency range of 7.5–10.5 GHz using a vector network analyzer (Agilent Technology E5071C), and two X-band standard gain horn antennas (Model: 16240, Flann Microwave Instruments) are used to transmit the EM wave on the sample absorber sheet and to receive both the reflected and the transmitted signals to measure the absorption rate at normal incidence.

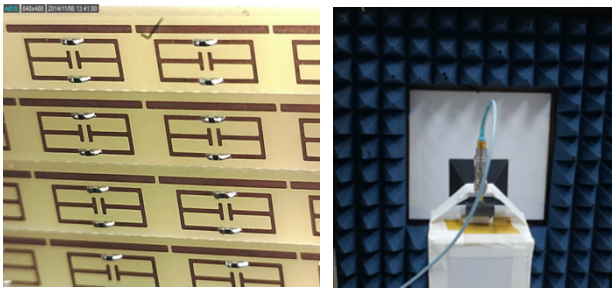

(a) (b)

Figure 9. (a) Photographs of the fabricated prototype absorber strip samples and (b) absorption measurement set up with horn antenna

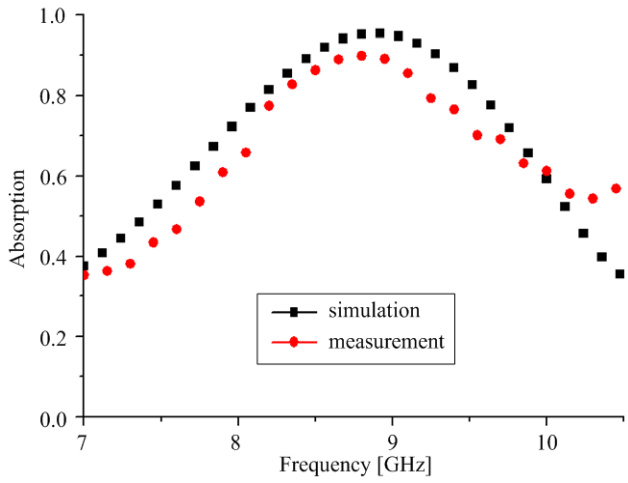

Figure 10. Calculated and measured absorption rate of the MM absorber at normal incidence

A microwave absorbing material is placed between the horns and surrounding the sample sheet, to eliminate unwanted edge scattering. The calculated and measured frequency-dependent absorption rates using the measured magnitudes of the S_{11} and S_{21} parameters of the planar arrayed unit cells are plotted as shown in Figure 10. These results show that the experimental peak absorption rate is slightly lower than that demonstrated by the simulated results. The experimental results show that the fabricated MM absorber sample exhibits a peak absorption rate of 91% at 8.87 GHz, and the FWHM bandwidth is approximately 2.8 GHz.

6. Conclusions

We have designed, simulated, and experimentally verified a new type of a backplane-less MM absorber configuration. A metallic pattern layer of the proposed absorber is designed in parallel to the incident wave propagation direction. The main effects of the lump resistor on the ELC resonator are lowering the Q-factor of the resonator and exhibiting a negative effective permeability ($\mu_{eff} < 0$). We have fabricated a prototype absorber with a planar array of 33 × 70 unit cells and experimentally verified the performance of the proposed absorber. The experimental results demonstrate that the composite MM absorber comprising an ELC resonator loaded with lumped resistors and a cut-wire strip configuration exhibits a wider absorption bandwidth than the previously designed MM absorber with an ELC resonator. The results of our study show that the design of the proposed absorber configuration can be easily extended to the design of more compact, thinner backplane-less planar absorbers for mm-wave and terahertz-frequency applications.

REFERENCES

[1] H. Tao, C. M. Bingham, D. Pilon, K. Fan, A. C. Strkwerda, D. Shrekenhammer, W. J. Padilla, X. Zhang, and R. D. Averitt, "A dual band terahertz metamaterial absorber," J. Appl. Phys. D, vol. 43, pp. 225102–225106, 2010.

[2] M. Li, H.-L.Yang, X. -W. Hou, Y. Tian, and D.-Y. Hou "Perfect metamaterial absorber with dual bands," Progress in Electromagnetics Research, vol.108, pp. 37–49, 2010.

[3] J., Lee, and S., Lim, "Bandwidth-enhanced and polarization-insensitive metamaterial absorber using double resonance," Electron. Lett., vol. 47, 2011, pp. 8–9.

[4] Y. Cheng, H. Yang, Z. Cheng, and N. Wu, "Perfect metamaterial absorber based on a split-ring-cross resonator," J. Appl. Phys. A, vol. 102, pp. 99–103, 2010.

[5] X.-J. He, Y. Wang, J. Wang, T. Gui, and Q. Wu, "Dual-band terahertz metamaterial absorber with polarization insensitivity and wide incident angle," Progress In Electromagnetics Research, vol. 115, pp. 381–397, 2011.

[6] F. Bilotti, A. Toscano, K. B. Alici, E. Ozbay, and L. Vegini, "Design of miniaturized narrowband absorbers based on resonant-magnetic inclusions," IEEE Trans. on Electromagnetic Compatibility, vol. 53, pp. 63–72, 2011.

[7] Y. Cheng and H. Yang, "Design, simulation, and

measurement of metamaterial absorber," Microwave Opt. Tech. Lett., vol.52, pp. 877–880, 2010.

[8] H. Tao, C. M. Bingham, D. Pilon, K. Fan, A. C. Strikwerda, D. Shrekenhamer, W. J. Padilla, X. Zhang, and R. D. Averitt, "A dual band terahertz metamaterial absorber," J. of Phys. D: Appl. Phys., vol. 43, pp. 225102–225106, 2010.

[9] X. Shen, T. J. Cui, J. Zhao, H. F. Ma, W. X. Jiang, and H. Li "Polarization-independent wide-angle triple-band metamaterial absorber," Optic Express, vol. 19, pp. 9401–9407, 2011.

[10] H. Li, L. H. Yuan, B. Zhou, X. P. Shen, Q. Cheng, and T. J. Cui, "Ultrathin multiband gigahertz metamaterial absorbers," J. Appl. Phys., vol.110, pp. 0149091–0149098, 2011.

[11] B. Zhu, Z. Wang, C. Huang, Y. Feng, J. Zhao, and T. Jiang, "Polarization insensitive metamaterial absorber with wide incident angle," Progress In Electromagnetics Research, vol. 101, pp. 231–239, 2010.

[12] H. Lee, "Design of metamaterial absorber based on resonant magnetic inclusion," Proceeding of ISAP2012, Nagoya, Japan, pp. 1501–1504, Oct. 2012.

[13] Y. Z. Cheng, Y. Wang, Y. Nie, R. Z. Gong, X. Xiong, and X. Wang, "Design, fabrication and measurement of a broadband polarization-insensitive metamaterial absorber based on lumped element," J. Appl. Phys., vol. 111, pp. 0449021–04490214, 2012.

[14] D. Schurig, J. J. Mock, and D. R. Smith, "Electric-field-coupled resonators for negative permittivity metamaterials," Appl. Phys. Lett., vol. 88, 2006, pp. 0411091–0411093.

[15] W. J. Padilla, M. T. Aronsson, C. Highstrete, M. Lee, A. J. Taylor, and R. D. Averitt, "Electrically resonant terahertz metamaterials: theoretical and experimental investigations," Phys. Rev. B, vol. 75, 2007, pp. 0411021–0411024.

[16] Y. Liu, N. Fang, D. Wu, C. Sun, and X. Zhang, "Symmetric and antisymmetric modes of electromagnetic resonators," Appl. Phys. A, vol. 87, 2007, pp. 171–174.

[17] R. A. Depine, and A. Lakhtakia, "A new condition to identify isotropic dielectric-magnetic materials displaying negative phase velocity," Microwave Opt. Tech. Lett., vol. 41, pp. 315–316, 2004.

[18] H. -M. Lee, H. -S. Lee, "Switchable resonant mode behavior of an electric-inductive-capacitive resonator", IEEE Int'l Syp. Antennas and Propagation, pp. 1362- 1363, Jun. 2013.